



Cationic Au(I) complexes with aryl-benzothiazoles and their antibacterial activity

Jenny Stenger-Smith, Indranil Chakraborty, Pradip K. Mascharak*

Department of Chemistry, University of California, Santa Cruz, CA 95064, United States

ARTICLE INFO

Keywords:

Aryl-benzothiazoles
Gold(I) complexes
Antibacterial activity
Gram-negative bacteria
Skin and soft tissue infection (SSTI)

ABSTRACT

Two cationic Au(I) complexes derived from aryl-benzothiazoles, namely $[(PPh_3)Au(pbt)](OTf)$ (**1**) and $[(PPh_3)Au(qbt)](OTf)$ (**2**) (where pbt = 2-(pyridyl)benzothiazole and qbt = (quinoly)benzothiazole, and OTf^- = trifluoromethanesulfonate anion), have been synthesized and structurally characterized by X-ray crystallography. Both complexes exhibit strong antibacterial effects against Gram-negative bacteria such as *Acinetobacter baumannii* and *Pseudomonas Aeruginosa*. Results of examination of the reactions of **1** and **2** indicate that these cationic Au(I) complexes rapidly cross the bacterial membrane and exert drug action by disrupting cellular function(s) through binding of cytosolic thiol-containing peptides (such as glutathione) and proteins to the highly reactive $(PPh_3)Au^+$ intermediate formed upon in situ dissociation of pbt or qbt.

1. Introduction

Rapid emergence of antibacterial resistance to common antibiotics has raised alarm in hospitals around the globe. Infections and diseases that were thought to be well controlled by antibiotics are reappearing with resistance to traditional drug therapies [1]. In parallel, other microorganisms such as parasites, fungi, and viruses are also exhibiting similar characteristics [2]. Many resistant strains have appeared in hospitals where antibiotics are being used and administered as routine procedures [3]. The once life-saving drugs like β -lactams that doctors relied upon to keep many bacterial infections at bay are now completely ineffective [4]. Unfortunately, the pace at which new antibiotics are emerging in the market is not nearly fast enough to combat such resistance [5].

Although gold compounds have been used in medicine for centuries, interest in such compounds was noticeably intensified following the discovery by Robert Koch who showed that $K[Au(CN)_2]$ had activity against *Mycobacterium tuberculosis*, the causative agent of tuberculosis [6,7]. Shortly after this discovery, reports on gold compounds as anticancer, antimicrobial, and antiarthritic agents started appearing in scientific literature and such research led to several gold drugs for commercial use [6–10]. Additional investigation into new gold compounds for clinical use was however greatly diminished following the discovery of antibiotics. Now that resistance is on the rise and the discovery of new antibiotics is comparatively slow [5], reexamination of the bioactivity of new gold compounds could be very relevant.

In recent years a relatively large number of Au(I) compounds have

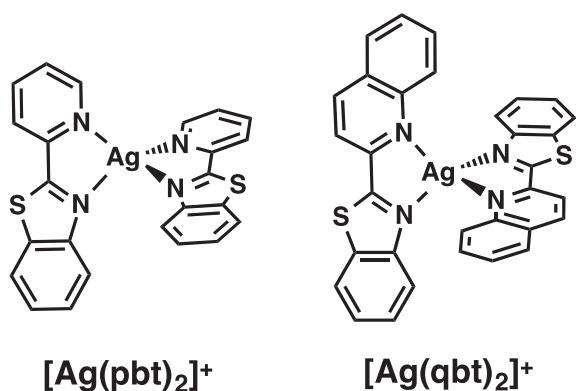
been synthesized and studied in vitro. The accumulation and in-depth analysis of such data have led scientists to infer that the types of ligands in the gold compounds play a significant role in the effectiveness of the compounds toward eradication of specific bacteria [6]. Interestingly, compounds independently used as drugs, when used as ligands to Au(I), lead to new gold compounds exhibiting improved antibacterial efficacy. Positively-charged species are in general more effective in associating with mostly electronegative bacterial cell walls [11]; close interactions between the cell wall and drug molecules lead to interruptions in various cellular pathways that often result in microbial death.

For some time, we have been exploring the antibacterial properties of heavy metal complexes derived from benzothiazoles, a class of antibacterial and antifungal drugs [12,13]. Our work in such pursuit have shown that Ag(I) complexes of benzothiazole-type ligands act as antimicrobial agents [14]. In these complexes, 2-(pyridyl)benzothiazole (pbt) and 2-(quinoly)benzothiazole (qbt) are bound to the Ag(I) center as bidentate *N,N*-coordinated fashion to give rise to tetrahedral geometry (Scheme 1). The overall positive charge of these complexes presumably leads to stronger interactions with the bacterial cell walls and give rise to their antibacterial activity. These results prompted us to explore the coordination characteristics of pbt and qbt to Au(I) centers and the antibacterial activity of the Au(I) complexes derived from them.

In this account we report the synthesis, spectroscopy, and structural characterization of two gold(I) compounds derived from pbt and qbt namely, $[(PPh_3)Au(pbt)](OTf)$ (**1**) and $[(PPh_3)Au(qbt)](OTf)$ (**2**). As shown in Figs. 2 and 3, both ligands bind as monodentate *N*-donors to the Au(I) center. The other ligand in both complexes is

* Corresponding author.

E-mail address: pradip@ucsc.edu (P.K. Mascharak).



Scheme 1. Structures of the Ag complexes derived from pbt and qbt.

triphenylphosphine. The antibacterial properties of **1** and **2** against two Gram-negative bacteria namely, *Acinetobacter baumannii* and *Pseudomonas aeruginosa* have been evaluated using a skin and soft tissue infection (SSTI) model previously developed in our laboratory.

2. Experimental methods

2.1. Materials and methods

All reagents and solvents were of commercial grade and used without further purification. $(\text{PPh}_3)\text{AuCl}$ and AgOTf were procured from Sigma. The ligands pbt [15] and qbt [16] were synthesized according to reported procedures. FTIR, UV–Vis, and emission spectra were obtained using Perkin-Elmer Spectrum-One, Varian Cary 50, and Agilent Cary Eclipse spectrophotometers respectively. The ^1H -, ^{19}F and ^{31}P NMR spectra of the ligands and the complexes were recorded using a Varian Unity Inova 500 MHz instrument at 298 K.

2.2. Synthesis of complexes

2.2.1. Synthesis of $[(\text{PPh}_3)\text{Au}(\text{pbt})](\text{OTf})$ (**1**)

To a solution of AgOTf (54.8 mg, 0.213 mmol) in 10 mL of methanol was added a solution of $(\text{PPh}_3)\text{AuCl}$ (100.5 mg, 0.203 mmol) in 15 mL of chloroform. After stirring for 30 min the white AgCl precipitate was filtered through a bed of celite. To the filtrate was added a solution of pbt (43.1 mg, 0.203 mmol) in 10 mL of chloroform and the mixture was set to reflux for 18 h. The solution was again filtered through celite to remove traces of black particles. The volume of the filtrate was then reduced to approximately 4 mL and 15 mL of hexane was added. The white solid thus formed was collected by filtration and dried in vacuo (131.0 mg, 78.6% yield). Layering hexanes over a dichloromethane (CH_2Cl_2) solution of this solid afforded colorless crystals of **1**. Anal. Calcd for $\text{C}_{31}\text{H}_{23}\text{AuN}_2\text{O}_3\text{PS}_2\text{F}_3$: C, 45.37; H, 2.83; N, 3.41; found: C, 45.48; H, 2.79; N, 3.37. IR (KBr, cm^{-1}): 3468 (w), 3056 (w), 1459 (w) 1436 (m), 1267 (s), 1154 (m), 1032 (m), 763 (m), 695 (m), 546 (m). ^1H NMR (CDCl_3 , ppm): 8.62 (d, 1H), 8.40 (d, 1H), 8.25 (t, 1H), 8.12 (d, 1H), 8.01 (d, 1H), 7.83 (t, 1H), 7.63–7.55 (m, 17H). ^{31}P NMR (CDCl_3 , ppm from PPh_3): 35.90.

2.2.2. Synthesis of $[(\text{PPh}_3)\text{Au}(\text{qbt})](\text{OTf})$ (**2**)

The same procedure as above using qbt as the ligand. Complex **2** was isolated as a light yellow solid (60.1 mg, 75.0%). Layering hexanes over a solution of **2** in dichloromethane afforded pale yellow crystals of $[(\text{PPh}_3)\text{Au}(\text{qbt})](\text{OTf})$. Anal. Calcd for $\text{C}_{35}\text{H}_{25}\text{AuN}_2\text{O}_3\text{PS}_2\text{F}_3$: C, 48.28; H, 2.89; N, 3.22; found: C, 48.02; H, 2.91; N, 3.12. IR (KBr, cm^{-1}): 3436 (w), 3056 (w), 1436 (w), 1263 (s), 1156 (m), 1031 (m), 762 (m), 696 (m), 545 (m). ^1H NMR (CDCl_3 , ppm): 8.76 (d, 1H), 8.52 (d, 1H) 8.23 (d, 1H), 8.19 (d, 1H), 8.06 (d, 1H) 7.69–7.53 (m, 19 H) 7.46 (t, 1H).

2.3. X-ray crystallography

Colorless and light yellow block-shaped crystals of complexes **1**. $0.05\text{CH}_2\text{Cl}_2$ and **2** respectively were obtained by recrystallization through diffusion of hexanes into their dichloromethane (CH_2Cl_2) solutions. In case of **1**, a suitable crystal was selected and mounted on a Bruker D8 Quest diffractometer equipped with PHOTON II detector operating at $T = 298$ K. Data were collected with ω shutterless scan technique using graphite monochromated Mo-K α radiation ($\lambda = 0.71073$ Å). In case of **2**, a suitable single crystal was selected and mounted on a Bruker APEX-II CCD diffractometer with graphite monochromated Mo-K α radiation ($\lambda = 0.71073$ Å). In this case the crystal was also kept at $T = 298$ K during data collection and unit cell determination. Data were measured using ω scan technique. The total number of runs and images for both data collections was based on the strategy calculation from the program APEX3 (Bruker) [17]. The maximum resolution achieved was $\theta = 28.4^\circ$ for **1** and $\theta = 24.2^\circ$ for **2**. Cell parameters were retrieved using the SAINT (Bruker) software [18] and refined using SAINT (Bruker) on 9525 reflections for **1** and on 8496 reflections for **2**. Data reduction was performed using the SAINT (Bruker) software, which corrects for Lorentz polarization. The final completeness is 99.6% out to 28.4° in θ for **1** and 98.8% out to 24.2° in θ for **2**. Multi-scan absorption corrections were performed with both data sets using SADABS 2016/2 and SADABS 2014/5 respectively for **1** and **2** [19]. The absorption coefficient for **1** is 4.88 mm^{-1} and for **2** is 4.29 mm^{-1} . Minimum and maximum transmissions for **1** are 0.499 and 0.746 and the corresponding values for **2** are 0.573 and 0.745. The structures of **1** and **2** were solved in the space group C2/c (No. 15) and Pbcu (No. 61) respectively by intrinsic phasing using the ShelXT [20] structure solution program and refined by full matrix least squares on F^2 using version 2016/6 of ShelXL [21]. All non-hydrogen atoms were refined anisotropically in both cases. Hydrogen atom positions were calculated geometrically and refined using the riding model. In case of **1**, there are two crystallographically independent molecules within the asymmetric unit, while for **2** one full molecule is present in the asymmetric unit. Calculations and molecular graphics were performed using SHELXTL 2014 and Olex2 [22] programs. Crystal data and structure refinement parameters are included in Table 1 while the bond distances and angles are listed in Table 2.

Crystal data for complex **1** (CCDC 1824282) and **2** (CCDC 1824283) have been included in the Supplementary data section. These data can be obtained free of charge from The Cambridge Crystallographic Data Center via www.ccdc.cam.ac.uk/data_request.cif.

2.4. Bacterial studies

The SSTI model previously developed in our lab [23] was employed for antimicrobial studies. This uses a soft upper agar layer of evenly-dispersed bacterial “lawn” at the top of a nutrient rich bottom agar layer. Such arrangement allows the bacteria to move slowly into the bottom layer following the nutrient gradient, much like ditching of surface bacteria into the inner layers of skin and soft tissue. Different dilutions of *A. baumannii* and *P. aeruginosa* were employed to grow ideal lawns in these SSTI models. For *A. baumannii*, a frozen stock of bacteria was first streaked on an LB plate and incubated for 18 h. A single colony of bacteria was selected and grown in LB broth for another 18 h. The suspension was diluted with fresh LB until an A_{600} of 0.8 was reached. A batch of 100 mL of 0.8% (w/v) agar with 1% NaCl was prepared, autoclaved and cooled to 47°C before addition of 80 μL of the diluted bacterial suspension. This solution was gently vortexed and aliquots of 8 mL of it were spread evenly over the surface of six $100 \times 15\text{ mm}^2$ plates prepared with 20 mL of 1.5% (w/v) TSB agar (hard nutrient-rich layer). The plates were then incubated at 37°C for 2 h to facilitate adhesion of the bacteria to the nutrient-rich bottom layer and cell-to-cell contact. For *P. aeruginosa*, the same procedure was followed to prepare the SSTI model. Here, the bacterial suspension in LB medium was diluted to an A_{600} of 0.5 and 120 μL of it

Table 1
Crystal data and structure refinement parameters for **1** and **2**.

	1. 0.5 CH ₂ Cl ₂	2
Formula	C _{31.5} H ₂₄ ClF ₃ N ₂ O ₃ S ₂ PAu	C ₃₅ H ₂₅ F ₃ N ₂ O ₃ S ₂ PAu
<i>D</i> _{calc.} /g cm ⁻³	1.777	1.601
<i>μ</i> /mm ⁻¹	4.875	4.285
Formula weight	863.03	870.62
Color	Yellow	Yellow
Shape	Block	Block
<i>T</i> /K	298(2)	298(2)
Crystal system	Monoclinic	Orthorhombic
Space group	C2/c	Pbca
<i>a</i> /Å	47.014(2)	9.780(2)
<i>b</i> /Å	8.7125(4)	22.679(5)
<i>c</i> /Å	36.5473(18)	32.560(7)
<i>α</i> /°	90	90
<i>β</i> /°	120.4450(10)	90
<i>γ</i> /°	90	90
<i>V</i> /Å ³	12,905.9(11)	7222(3)
<i>Z</i>	8	8
Wavelength/Å	0.71073	0.71073
Radiation type	Mo-Kα	Mo-Kα
2 θ _{min} /°	5.674	4.706
2 θ _{max} /°	56.712	48.376
Measured Refl.	123,645	40,970
Independent Refl.	16,063	5736
Reflections used	12,893	4345
<i>R</i> _{int}	0.0386	0.0487
Parameters	802	424
^a GooF	1.125	1.070
^c wR ₂	0.1120	0.1008
^b R ₁	0.0492	0.0428

^a GOF = $[\sum[w(F_o^2 - F_c^2)^2]/(N_o - N_v)]^{1/2}$ (*N*_o = number of observations, *N*_v = number of variables).

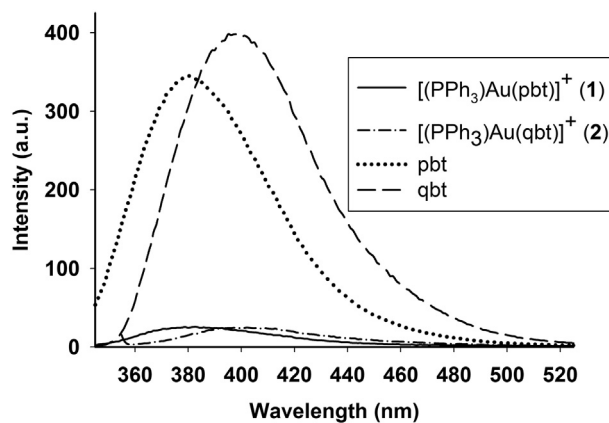
^b $R_1 = \sum||F_o| - |F_c||/\sum|F_o|$.

^c $wR_2 = [(\sum w(F_o^2 - F_c^2)^2)/\sum|F_o|^2]^{1/2}$.

Table 2
Selected bond distances (Å) and angles (°) for complex **1**.CH₂Cl₂ and **2**.

Complex 1			
Molecule 1			
Au(1)-P(1)	2.227(13)	Au(1)-N(2)	2.116(4)
P(1)-C(13)	1.810(6)	N(2)-C(6)	1.292(7)
P(1)-Au(1)-N(2)	166.50(15)	Au(1)-P(1)-C(13)	113.77(19)
Au(1)-P(1)-C(19)	110.91(18)	Au(1)-P(1)-C(25)	112.66(19)
C(13)-P(1)-C(25)	107.5(3)	Au(1)-N(2)-C(6)	125.8(4)
Au(1)-N(2)-C(12)	122.3(4)	C(6)-S(1)-C(7)	90.4 (3)
Molecule 2			
Au(2)-P(2)	2.221(14)	Au(2)-N(4)	2.112(6)
P(2)-C(29)	1.816(6)	N(4)-C(36)	1.319(9)
P(2)-Au(2)-N(4)	163.26(19)	Au(2)-P(2)-C(49)	113.5(2)
Au(2)-P(2)-C(42)	110.08(19)	Au(2)-P(2)-C(55)	113.7(2)
C(55)-P(2)-C(49)	107.9(3)	Au(2)-N(4)-C(36)	124.6(6)
Au(2)-N(4)-C(42)	123.0(5)	C(37)-S(2)-C(36)	90.9 (4)
Complex 2			
Au(1)-P(1)	2.303(18)	Au(1)-N(2)	2.218(5)
P(1)-C(17)	1.881(7)	N(2)-C(10)	1.359(8)
P(1)-Au(1)-N(2)	161.20(15)	Au(1)-P(1)-C(17)	117.0(2)
Au(1)-P(1)-C(29)	110.2(2)	Au(1)-P(1)-C(23)	111.6(2)
C(17)-P(1)-C(23)	105.5(3)	Au(1)-N(2)-C(10)	121.9(4)
Au(1)-N(2)-C(11)	125.5(4)	C(10)-S(1)-C(16)	91.1(3)

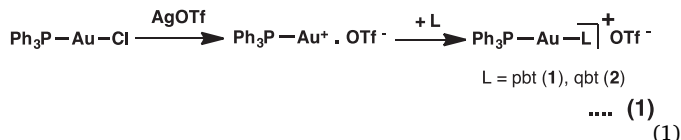
was added to the 100 mL of soft agar solution. The SSTI models were prepared using 7 mL of the soft agar solution spread evenly over the surface of the hard agar layer. After preparation the plates and initial incubation of 2 h, the KBr pellets containing the Au(I) complexes were placed on all SSTI models and incubated for 18 h to evaluate the anti-bacterial activity of the Au(I) compounds.

**Fig. 1.** Emission spectra of **1** (λ_{ex} 330 nm) and **2** (λ_{ex} 350 nm) compared to free ligands in dichloromethane (λ_{ex} 310 and 335 nm for pbt and qbt respectively).

3. Results and discussion

3.1. Synthesis and spectroscopic properties

The addition of 1.05 eq of AgOTf to (PPh₃)AuCl afforded the highly reactive ion-pair AuPPh₃⁺.OTf⁻ [24] which was then further reacted with 1 eq of pbt or qbt under refluxing condition to obtain **1** and **2** respectively (Eq. (1)).



The IR spectra of both **1** and **2** show a strong band around 1265 cm⁻¹ corresponding to the presence of the OTf⁻ counter ion. Both complexes exhibit significant luminescence quenching in organic solvents when compared to the free ligand at the same concentration (Fig. 1). Similar partial quenching has been observed with [Ag(pbt)₂]BF₄ and [Ag(qbt)₂]BF₄ [14]. However, in the Ag(I) complexes, both ligands are bound in a bidentate fashion while in **1** and **2**, the ligands act as monodentate N-donors. The wavelength of emission for **1** and **2** are 380 nm and 400 nm respectively which are the wavelengths of emission for the corresponding free ligands pbt and qbt. A close scrutiny of the literature reveals that both the singlet and triplet excited states of Ag(I) and Au(I) complexes of similar coordination structures essentially possess ligand-centered $\pi\pi^*$ character with negligible metal-to-ligand charge transfer (MLCT) contribution, and the excited triplet state mostly decay through non-radiative channels [14,25]. These characteristics presumably lead to significant luminescence quenching observed with the pbt and qbt complexes.

3.2. Crystal structure description

Single crystal analysis reveals that complexes **1** and **2** are isostructural with respect to coordination at the Au center; in both cases the Au center resides in a linear N-Au-P coordination environment. For complex **1**, the asymmetric unit contains two crystallographically independent molecules. The perspective view with atom labeling scheme for the two structures are shown in Figs. 2 and 3. The N(benzothiazole)-Au-P angles in complexes **1** and **2** are 164.88(17) and 161.20(15)° respectively. Steric bulk of the qbt ligand leads to lengthening of both the average Au-N(benzothiazole) distance (2.114(5) Å for **1** vs. 2.218(5) Å for **2**) and the average Au-P distance (2.224(14) for **1** vs. 2.303(18) Å for **2**) in complex **2**. Although Cambridge structural database revealed several crystal structures with N-Au-P coordination mode, a representative structurally analogous complex namely, [(py)Au

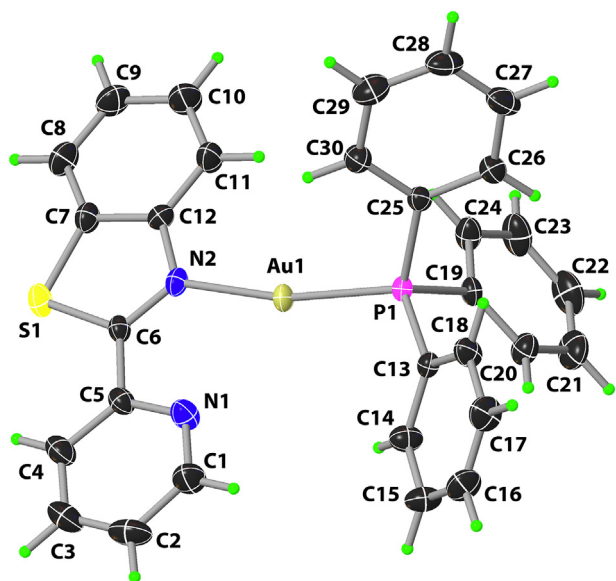


Fig. 2. Perspective view of the cation of complex 1 with the atom-labeling scheme. The thermal ellipsoids are shown at 50% probability level. Only one of the two crystallographically independent molecules in the asymmetric unit is shown.

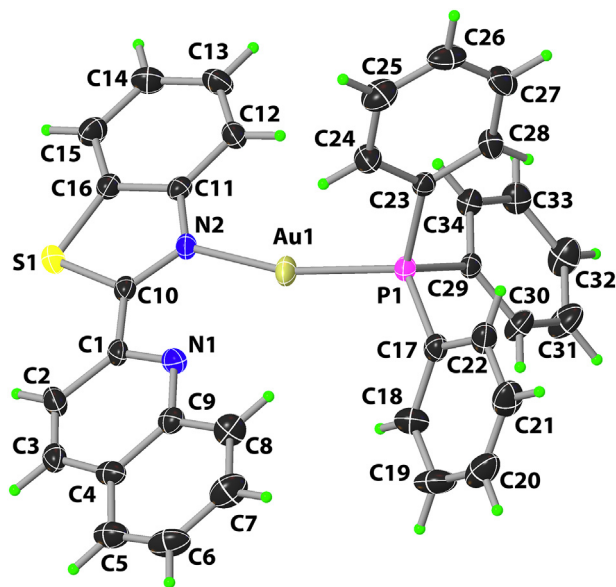


Fig. 3. Perspective view of the cation of complex 2 with the atom-labeling scheme. The thermal ellipsoids are shown at 50% probability level.

(PPh₃)]BF₄ [26] (where py = pyridine), was chosen to compare its crucial metric parameters with those of the present two complexes. In [(py)Au(PPh₃)]BF₄, the N(py)-Au and Au-P bond lengths are 2.073(3) Å and 2.2364(8) Å respectively. These distances are quite comparable to those noted for 1 and 2. Interestingly, the N-Au-P angle in [(py)Au(PPh₃)]BF₄ is 178.09(8)°, more close to a linear geometry, unlike 1 and 2. In the present two structures, both pbt and qbt exhibit excellent planarity with mean deviations of 0.024(3) and 0.090(4) Å respectively. The packing patterns for both structures revealed no classical hydrogen bonding interactions. However, several weak non-bonding contacts consolidated the extended lattice of these two complexes (Supplementary data, Figs. S1–S3).

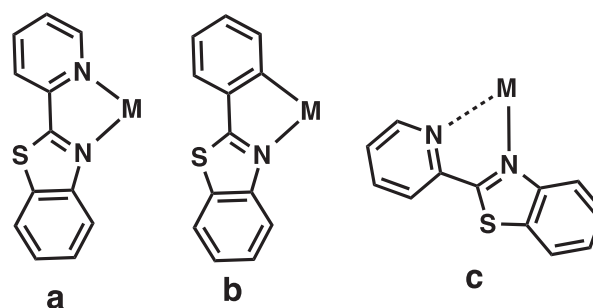


Fig. 4. Different modes of binding of pbt and aryl-benzothiazole.

3.3. Binding modes of 2-(aryl)benzothiazoles

2-aryl or 2-pyridyl substituted benzothiazole type ligands (like pbt and qbt) typically exhibit bidentate binding modes when coordinated to d¹⁰ metal center. This can occur through the N-atom of the benzothiazole moiety and either the N-atom of the 2-pyridyl fragment [14] or C-atom of the 2-aryl portion [27] of the ligand (Fig. 4a and b respectively). Similar *N,N*-binding of pbt and qbt has been noted in complexes with low-spin d⁶ metal centers such as Mn(I) and Re(I) [16,28–30]. In all cases, the ring S-atom does not coordinate.

When this type of ligands were employed for coordination to Au(I) centers in this research, the ligands failed to coordinate as bidentate ligands. Attempts to coordinate pbt and qbt to Au(I) center invariably afforded linear 2-coordinated complexes 1 and 2. Despite strong affinity of Au(I) to S-donors, both ligands are coordinated to the metal center through the N-atom of the benzothiazole (N(2)) moiety. This is in agreement with results from similar studies exploring the binding modes of Au(I) to ligands with electronically similar N and S (or N) donor atoms [31,32]. Mono-substituted binding mode of these types of ligands (leading to linear complexes) also arises from steric hindrance arising from the ligand itself [25]. Both the present complexes deviate from linearity; the P-Au-N angle of 1 and 2 are 166.50° and 161.22° respectively (Figs. 2 and 3, Table 2). Also, the P-Au-N angle of 2 with sterically more encumbered qbt ligand deviates more from linearity compared to 1.

It is important to note that in 1 and 2, the N atom of the pyridine/quinolyl moiety (N(1)) is facing the metal center, but not bound. Results of previous studies on the structures and ground state optimized geometries of the free ligands [14] have demonstrated that although the structure with the pyridyl-N and benzothiazole-N atom *anti* to each other is lower in energy, in all cases both pbt and qbt bind metal ions as the N–N *syn* structural isomer [14,16,28–30]. The pyridine fragment in these cases rotates to present its N center to be available for coordination in a N–N *syn* fashion (Scheme 1 and Fig. 4a). In 1 and 2, *this rotation of the aryl ring also occurs*, but the pyridyl-N or the quinolyl-N does not bind to the metal center. However, in both cases, significant interactions between this N-atom and the Au(I) center is observed in 1 [Au(1)–N(1), 2.713 Å] and 2 [Au(1)–N(10), 2.710 Å] (Fig. 4c) which is in agreement with other gold(I) compounds of similar structure [33].

3.4. Antibacterial studies

Antibacterial studies were done using the skin and soft tissue infection (SSTI) model previously developed in this laboratory [23]. This model mimics the gradual penetration of bacteria deeper into the skin using a two-layer agar system which has a soft, evenly dispersed bacterial lawn on the top and a nutrient-rich bottom layer. The gradient causes the bacteria to slowly migrate from the thin top layer to the nutrient-rich bottom layer much like the way an infection of the skin would proceed.

Both complexes and the corresponding ligands were tested *in vitro* for their bactericidal activity against the Gram-negative bacterium *A.*

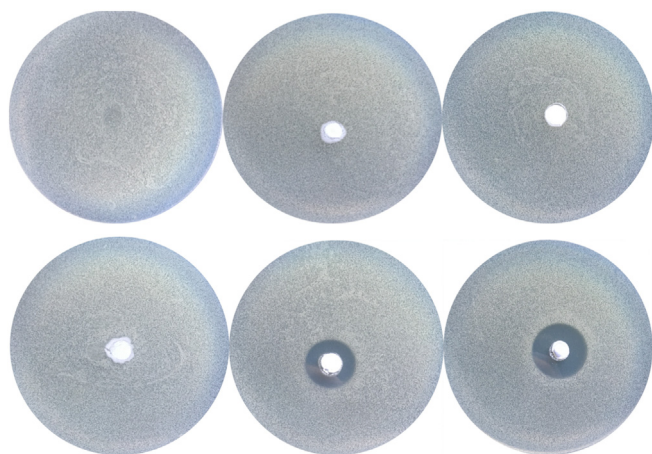


Fig. 5. Bacterial lawns after 18 h incubation with KBr pellets of KBr, pbt and qbt (top panel, left to right) and $(\text{PPh}_3)\text{AuCl}$, **1**, and **2** (bottom panel, left to right).

baumannii. This bacterium has shown multidrug-resistance in hospitals around the world and at present poses serious threat to human health. In addition to resistance traits carried on mobile genetic elements, *A. baumannii* also forms biofilms rapidly as defensive barriers. In addition, *A. baumannii* infections are a primary concern to military personnel injured by gun fire and improvised explosive devices (IEDs) in the battlefields of Afghanistan and Iraq [34]. With a limited pipeline of new antibiotics being developed for Gram-negative bacteria, new therapies are in high demand, especially for this pathogen. In the present work, a gold control (the neutral starting material PPh_3AuCl) was also used to show how the ligands and the cationic nature of **1** and **2** affect the ability of the Au(I) complexes to interact with the bacterial colonies. KBr pellets of similar weights containing 0.3 mol% of compounds were placed on the top of the bacterial lawn and incubated at 37 °C for 18 h. Circular zones of clearing were seen around the pellets containing **1** and **2**, but not around the pellets containing KBr, pbt, qbt or $(\text{PPh}_3)\text{AuCl}$ (Fig. 5). These results indicate that the two Au(I) complexes are better able to migrate and interfere with a large area of infection while the neutral gold compound exhibit no eradication of the bacteria on the SSTI model.

The antimicrobial activity of various drugs is highly dependent on their ability to permeate through the cell wall and interfere with cellular pathways [9]. Most bacteria possess a slightly electronegative surface potential which allows cationic complexes to associate more readily with the bacterial membrane. If the drug molecules can easily form bonds with biomolecules either on the membrane or in the cytosol, the efficacy of the drug action is enhanced. For gold compounds this implies that the nature of the ligands bound to the Au(I) center, not just the amount of Au(I) present, plays an important role in their activity [35]. The neutral and very stable compound $(\text{PPh}_3)\text{AuCl}$ therefore exhibits no activity against *A. baumannii* while the more ligand exchangeable and cationic complexes **1** and **2** are very effective in eradicating bacterial loads throughout the entire “kill zone” of the 4 mm thick SSTI disk.

It is important to note that although **1** and **2** exhibited high level of antibacterial activity (Fig. 5), no reduction of bacterial load was observed with $(\text{PPh}_3)\text{AuCl}$. Because pbt and qbt by themselves showed marginal antibacterial effect for *A. baumannii*, it is evident that effective interaction between the cationic gold complexes and bacterial cell membrane is the major cause of their bactericidal activity. Upon deligation of pbt or qbt from the metal center, a step that delivers these antibacterials to the cytosol, the highly reactive $\text{Ph}_3\text{PAu}^+\text{OTf}^-$ species could also exert strong antibiotic action through binding to membrane and/or cytosolic molecules [36]. In order to check whether **1** and **2** can bind to cellular SH-containing proteins and peptides (such as

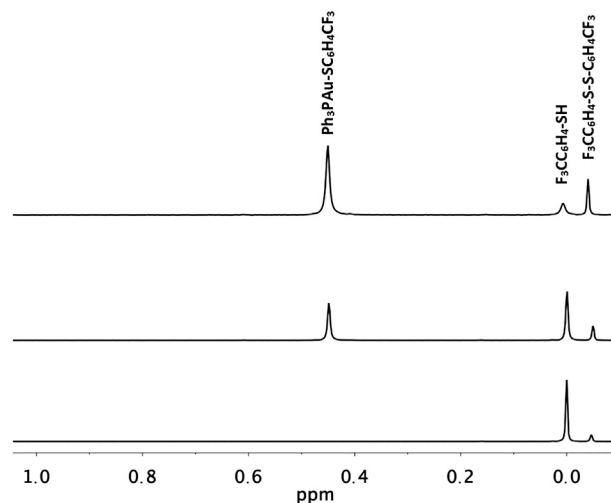


Fig. 6. ^{19}F NMR spectrum of the mixture of **1** and $\text{F}_3\text{CC}_6\text{H}_4\text{SH}$ (top trace), $\text{PPh}_3\text{Au-SC}_6\text{H}_4\text{CF}_3$ synthesized independently (middle trace) and $\text{F}_3\text{CC}_6\text{H}_4\text{SH}$ (bottom trace) in CDCl_3 . $\text{F}_3\text{CC}_6\text{H}_4\text{S-SC}_6\text{H}_4\text{CF}_3$ was present in the thiol as an impurity.

glutathione) present in the cytosol of the bacteria, **1** was treated with 1.2 equiv. of *p*-trifluoromethyl-benzene thiol ($\text{F}_3\text{CC}_6\text{H}_4\text{SH}$) and the reaction was followed by both ^{19}F and ^1H NMR spectroscopy (in CDCl_3). Interestingly, addition of the thiol to the Au(I) complex generated a new ^{19}F -peak at ~ 0.5 ppm downfield (with respect to $\text{F}_3\text{CC}_6\text{H}_4\text{SH}$) indicating binding of the thiol to the Ph_3PAu^+ unit (Fig. 6). The ^1H NMR spectrum of the reaction mixture clearly showed loss of pbt from the Au (I) center upon addition of the thiol. In an independent experiment, $\text{PPh}_3\text{Au-SC}_6\text{H}_4\text{CF}_3$ was synthesized by reacting $(\text{PPh}_3)\text{AuCl}$ with $\text{CF}_3\text{C}_6\text{H}_4\text{S}^-$ (prepared from $\text{CF}_3\text{C}_6\text{H}_4\text{SH}$ and Et_3N). The ^{19}F NMR spectrum of $\text{PPh}_3\text{Au-SC}_6\text{H}_4\text{CF}_3$ clearly confirmed its formation in the reaction between **1** and $\text{F}_3\text{CC}_6\text{H}_4\text{SH}$ (Fig. 6). In order to confirm that the PPh_3 ligand is not deligated in such reactions of **1** with SH-containing biomolecules, we allowed **1** to react with *N*-acetyl-L-cysteine methyl ester ($\text{HSC}_6\text{H}_{10}\text{NO}_4$) in CDCl_3 . The ^{31}P NMR spectrum of the reaction mixture clearly showed that the cysteine ester replaced pbt to form $\text{PPh}_3\text{Au-SC}_6\text{H}_{10}\text{NO}_4$ (Fig. 7). Complete absence of ^{31}P resonance of free PPh_3 in such reaction mixture confirms that no PPh_3 loss occurs upon reaction of **1** with the S-containing amino acid.

Deligation of pbt or qbt from both complexes by SH-containing

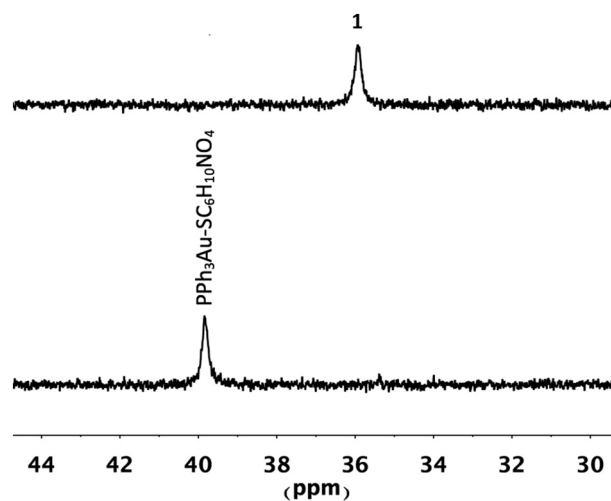


Fig. 7. ^{31}P NMR spectra of complex **1** and $\text{PPh}_3\text{Au-SC}_6\text{H}_{10}\text{NO}_4$ (formed upon addition of $\text{HSC}_6\text{H}_{10}\text{NO}_4$ to **1**) in CDCl_3 (the ppm values are w.r.t free PPh_3 in CDCl_3).



Fig. 8. Dramatic rise in luminescence upon addition of $\text{CF}_3\text{C}_6\text{H}_4\text{SH}$ to **2** in chloroform. Left: CHCl_3 solution of **2**; right: a mixture of **2** and $\text{CF}_3\text{C}_6\text{H}_4\text{SH}$ in CHCl_3 .



Fig. 9. Circular clearing ring in *P. aeruginosa* lawn upon application of **1**.

compounds can be readily observed by a dramatic increase in luminescence due to release of the strongly fluorescent ligands in solution. For example, when **2** was allowed to react with $\text{CF}_3\text{C}_6\text{H}_4\text{SH}$ in chloroform, a sharp increase in luminescence was observed (Fig. 8). Taken together, these observations suggest that complexes like **1** and **2** most likely generate the reactive Ph_3PAu^+ species (and free ligand) within the bacterial cell and disrupt the cellular mechanism(s) by binding to various biomolecules. Failure of free pbt and qbt in causing bacterial death could be attributed to their inability to cross cell membrane as well as their insolubility in aqueous media; complexes like **1** and **2** make such entry possible and possibly allow these ligands to exert their own antibacterial activity [12,13,37]. Lack of antibacterial activity of $(\text{PPh}_3)\text{AuCl}$ most possibly arises from its high stability and inability to pass through the cell membrane.

Finally, in order to test the antimicrobial activity of the present Au(I) complexes against a more common and invasive bacterium prevalent in nosocomial skin infections and burn injuries complex **1** was tested against *P. aeruginosa*. A KBr pellet containing 0.3 mol% of **1** was placed on a *P. aeruginosa* lawn and incubated at 37°C for 18 h. The large zone of killing (Fig. 9) confirmed that complex **1** is highly effective in eradication of *P. aeruginosa*. More studies toward application of these two Au(I) complexes to thwart skin and wound infections by several drug-resistant bacteria are in progress in this laboratory. The results will be reported in due time.

4. Conclusions

The strong antibacterial activity of two cationic Au(I) complexes reported here strongly suggest that gold compounds possess potential to combat skin and wound infections through topical applications. These types of Au(I) complexes derived from ligands that themselves exhibit antibacterial properties could be utilized in cases of drug-resistant bacterial infections. Both the ligand and the highly reactive

$\text{Ph}_3\text{PAu}^+\text{OTf}^-$ species could exert synergistic drug effects in such applications leading to better outcome. The present two complexes **1** and **2** provide proof-of-the-concept examples of such drug design approach.

Abbreviations

pbt	2-(pyridyl)benzothiazole
qbt	2-(quinolyl)benzothiazole
OTf^-	trifluoromethanesulfonate anion
LB	luria broth
TSB	tryptone soya broth
SSTI	skin and soft tissue infection
MLCT	metal-to-ligand charge transfer

Acknowledgements

Financial support from the NSF grant DMR-1409335 and a UCSC COR-SRG grant is gratefully acknowledged.

Appendix A. Supplementary data

Crystal data for complex **1** and complex **2** (in CIF format) and the packing diagrams (Figs. S1–S3). Supplementary data to this article can be found online at doi: <https://doi.org/10.1016/j.jinorgbio.2018.05.003>.

References

- [1] S.B. Levy, B. Marshall, Nat. Med. Suppl. 10 (2004) S122–S129.
- [2] C. Ash (Ed.), Trends in Microbiology, vol. 2, Elsevier, Cambridge, UK, 1994, pp. 341–422.
- [3] S.B. Levy, Sci. Am. 278 (1998) 46–53.
- [4] M. Barber, Lancet 2 (1948) 641–644.
- [5] A.R. Coates, G. Halls, Y. Hu, Br. J. Pharmacol. 163 (2011) 184–194.
- [6] D.G. Biljana, M.I. Djuran, Dalton Trans. 43 (2014) 5950–5969.
- [7] E.R. Tiekink, Gold Bull. 36 (2003) 117–124.
- [8] S.J. Berners-Price, A. Filipovska, Metallomics 3 (2011) 863–873.
- [9] S.H. van Rijjt, P.J. Sadler, Drug Discov. Today 14 (23–24) (2009) 1089–1097.
- [10] F. Mohr (Ed.), Gold Chemistry: Applications and Future Directions in the Life Sciences, Wiley-VCH Verlag GmbH & Co, Weinheim, Germany, 2009, pp. 283–319 (Ch. 6).
- [11] T.J. Beveridge, L.L. Graham, Microbiol. Rev. 55 (1991) 684–705.
- [12] B. Rajeeva, N. Srinivasulu, S.M. Shantakumar, Eur. J. Med. Chem. 6 (2009) 775–779.
- [13] K. Yamazaki, Y. Kaneko, K. Suwa, S. Ebara, K. Nakazawa, K. Yasuno, Bioorg. Med. Chem. 13 (2005) 2509–2522.
- [14] J. Stenger-Smith, I. Chakraborty, W.M.C. Sameera, P. Mascharak, Inorg. Chim. Acta 471 (2017) 326–335.
- [15] X. Chen, F.J. Femia, J.W. Babich, J. Zubieta, Inorg. Chim. Acta 314 (2001) 91–96.
- [16] J. Stenger-Smith, I. Chakraborty, S. Carrington, P. Mascharak, Acta Cryst (2017) C73.
- [17] Bruker, APEX 3, Bruker AXS Inc, Madison, Wisconsin, USA, 2014.
- [18] Bruker, SAINT, Bruker AXS Inc, Madison, Wisconsin, USA, 2012.
- [19] Bruker, SADABS, Bruker AXS Inc, Madison, Wisconsin, USA, 2014 and 2016.
- [20] G.M. Sheldrick, Acta Crystallogr., Sect. A: Found. Crystallogr. 71 (2015) 3–8.
- [21] G.M. Sheldrick, Acta Crystallogr. Sect. C 71 (2015) 3–8.
- [22] O.V. Dolomanov, L.J. Bourhis, R.J. Gildea, J.A.K. Howard, H. Puschmann, J. Appl. Crystallogr. 42 (2009) 339–341.
- [23] B.J. Heilman, J.S. John, S.R.J. Oliver, P.K. Mascharak, J. Am. Chem. Soc. 134 (2012) 11573–11582.
- [24] H. Duan, S. Sengupta, J.L. Petersen, N.G. Akhmedov, X. Shi, J. Am. Chem. Soc. 131 (34) (2009) 12100–12102.
- [25] C. Hsu, C. Lin, M. Chung, Y. Chi, G. Lee, P. Chou, C. Chang, P. Chen, J. Am. Chem. Soc. 133 (2011) 12085–12099.
- [26] S.E. Thwaite, A. Schier, H. Schmidbaur, Inorg. Chim. Acta 357 (2004) 1549–1557.
- [27] E. Lalinde, R. Lara, I.P. Lopez, M.T. Moreno, E. Alfaro-Arnedo, J.G. Pichel, S. Pineiro-Hermida, Chem. Eur. J. 24 (2018) 2440–2456.
- [28] I. Chakraborty, S.J. Carrington, G. Roseman, P.K. Mascharak, Inorg. Chem. 56 (2017) 1534–1545.
- [29] S.J. Carrington, I. Chakraborty, J.M.L. Bernard, P.K. Mascharak, Inorg. Chem. 55 (2016) 7852–7858.
- [30] S.J. Carrington, I. Chakraborty, J.M.L. Bernard, P.K. Mascharak, ACS Med. Chem. Lett. 5 (2014) 1324–1328.
- [31] M. Albrecht, K. Hubler, W. Kaim, Z. Naturforsch. 54b (1999) 1606–1608.
- [32] M. Munakata, S.G. Yan, M. Maekawa, M. Akiyama, S. Kitagawa, J. Chem. Soc. Dalton Trans. (1997) 4257–4262.
- [33] A. Ilie, C.I. Rat, S. Scheutzow, C. Kiske, K. Lux, T.M. Klapötke, C. Silvestru, K. Karaghiosoff, Inorg. Chem. 50 (2011) 2675–2684.
- [34] P.S. Gregory, D.A. Srinivasan, C. Murray, K. Moran, E. Hulten, J. Fishbain, D. Craft, S. Riddell, L. Linder, Clin. Infect. Dis. 44 (2007) 1577–1584.
- [35] F. Novelli, M. Recine, F. Sparatore, C. Juliano, Farmaco 54 (1999) 232–236.
- [36] S.J.B. Price, M.J. Dimartino, D.T. Hill, R. Kuroda, M.A. Mazid, P.J. Sadler, Inorg. Chem. 24 (1985) 3425–3434.
- [37] P.S. Jadav, A. Devprakash, G.P. Senthilkumar, Int. J. Pharm. Sci. Drug Res. 3 (2011) 1–7.